

Supporting Information

Establishment of the Interconnectivity among P(NDI2OD-T2)s in Organic Field-Effect Transistors by Non-Conjugated Crystalline Polymers

Hau-Ren Yang, Chun-Wei Pai, Han-Sheng Sun, Cuo Wu, Yu-Ying Lai*,
Shu-Chih Haw, Jey-Jau Lee, and Jin-Ming Chen

Table of Contents

1. General descriptions	2
2. Surface energy	3
3. Thermal analysis	4
4. Depth-profiling XPS	5
5. GIXS data	6
6. Statistical test in $-\sigma$	12
7. AFM height images	13
8. Device fabrication	14
9. Statistical data and transfer curves of OFETs	15
10. Reference	16

1. General descriptions

NMR. The NMR spectra were recorded on a AVIII HD 400 MHz, Bruker. Chemical shifts (δ) are reported in parts per million.

GPC. Gel permeation chromatography (GPC) was conducted at 40 °C in THF at a flow rate of 1.0 mL min⁻¹ on a JASCO instrument that was equipped with UV-vis and two Jordi DVB mixed-bed columns (250×10 mm; suitable for separating polymers with molecular weights from 10² to 10⁷ g mol⁻¹).

Thermal properties characterization. Thermogravimetric analysis (TGA) was recorded on a Q50, TA under nitrogen atmosphere at a heating rate of 10 °C/min. Differential scanning calorimetry (DSC) was conducted on a Q20, TA under nitrogen atmosphere at a scan rate of 10 °C/min. Tzero aluminum crucibles were used for loading the 3–5 mg samples.

Opto-electrical properties measurement. Film-type UV-vis absorption spectra were recorded on a model U-4100, *HITACHI* with wavelengths of incident beam varying from 1000 nm to 350 nm. Electrochemical cyclic voltammetry (CV) was conducted on a CH instruments electrochemical analyzer, CH614D. A carbon glass was used as the working electrode and a Ag/AgNO₃ electrode as the reference electrode, while 0.1 M tetrabutylammonium hexafluorophosphate in acetonitrile was the electrolyte. CV curves were calibrated using ferrocene as the standard, whose HOMO is set at -4.8 eV with respect to vacuum zero. The HOMO energy levels were obtained from the equation $\text{HOMO} = -(E_{ox} - E(\text{ferrocene}) + 4.8) \text{ eV}$. The LUMO levels were obtained from the equation $\text{LUMO} = -(E_{red} - E(\text{ferrocene}) + 4.8) \text{ eV}$.

Morphology characterization. Grazing incidence X-ray scattering (GIXS) was conducted at National Synchrotron Radiation Research Center (NSRRC) on beamline BL17A in Taiwan. The samples were irradiated with X-ray of $\lambda \sim 1.32 \text{ \AA}$ at a fixed incident angle of 0.2° and the GIXS patterns were recorded on a 2D image detector (Mar345 detector). Near edge X-ray absorption fine structure (NEXAFS) spectroscopy was carried out at National Synchrotron Radiation Research Center (NSRRC) on beamline BL20A in Taiwan. Atomic Force Microscopy (AFM) for surface topography was investigated by a Veeco diInnova AFM with standard tips (Tapping mode; L, 225 μm ; FREQ, 75 MHz; k, 2.8 N/m).

2. Surface energy

Surface energy was evaluated through Owens-Wendt equation (Eq. 1) with deionized water and glycerol as the liquid pair.

$$\sqrt{\gamma_s^d \gamma_L^d} + \sqrt{\gamma_s^p \gamma_L^p} = \frac{1}{2} (\gamma_L^d + \gamma_L^p) (1 + \cos \theta) \quad \text{Eq. (1)}$$

where γ_L^d and γ_L^p are the dispersion component and polar component of a liquid. γ_s^d and γ_s^p are those terms for a solid, such as a polymer film and the sum gives rise to surface energy γ_s .

γ_L^d and γ_L^p of deionized water are taken as 26.4 mJ m^{-2} and 46.4 mJ m^{-2} , respectively. γ_L^d and γ_L^p of glycerol are taken as 37.0 mJ m^{-2} and 26.4 mJ m^{-2} , respectively.

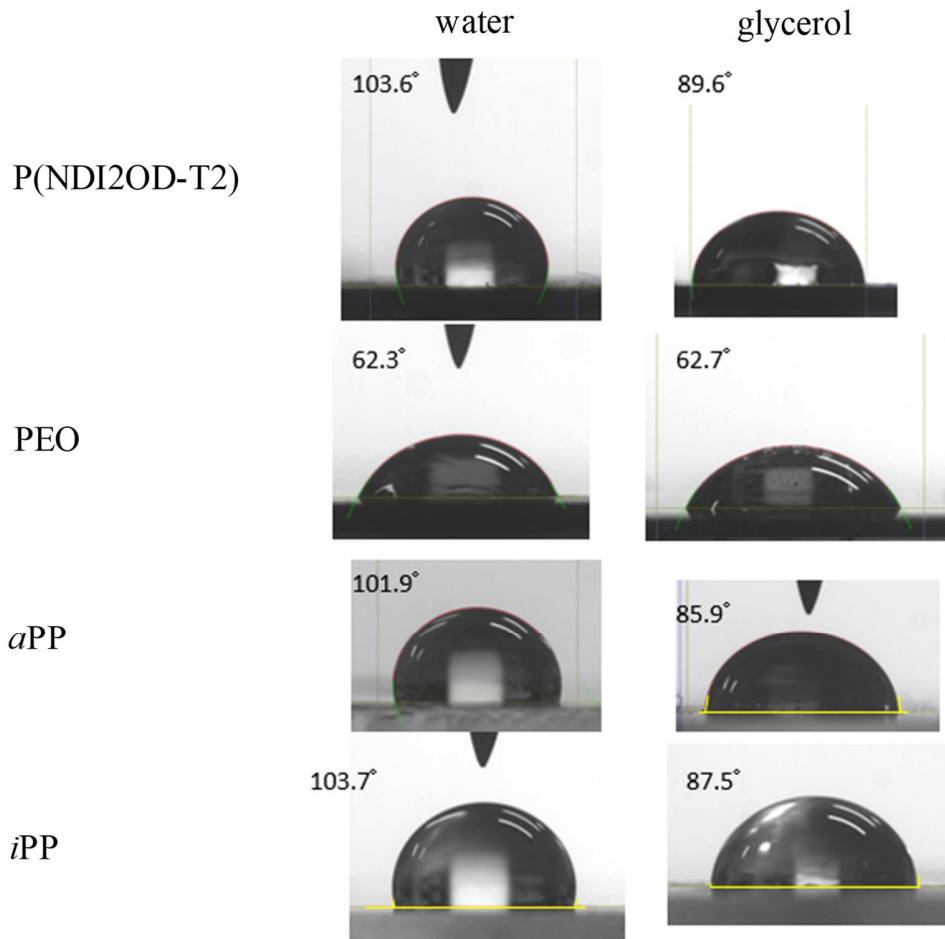


Figure S1 Contact angles of P(NDI2OD-T2), PEO, aPP, and iPP.

3. Thermal analysis

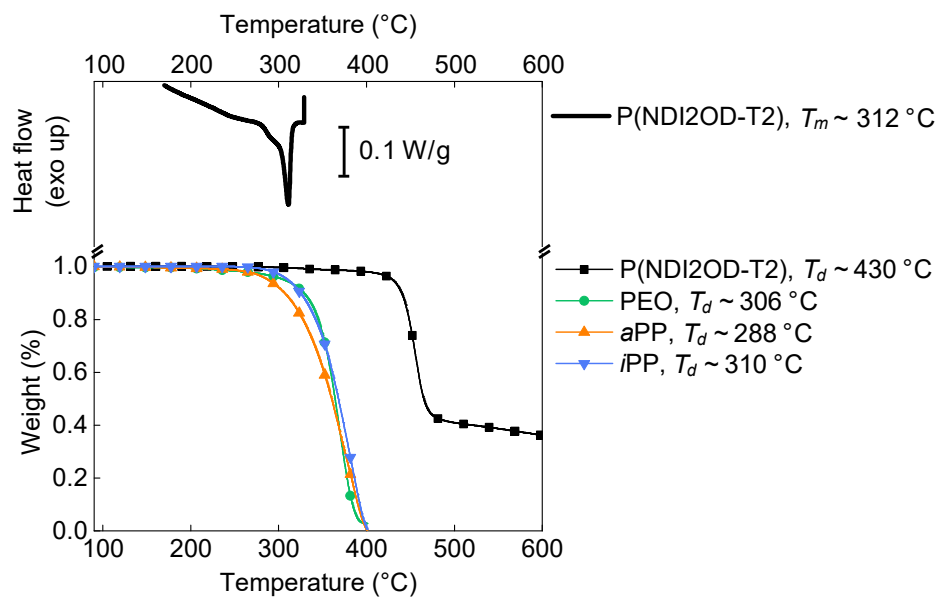


Figure S2. Differential scanning calorimetry and thermogravimetric analysis. The extracted melting point (T_m) and decomposition temperature (T_d , 5% weight loss) are indicated in the legends.

4. Depth-profiling XPS

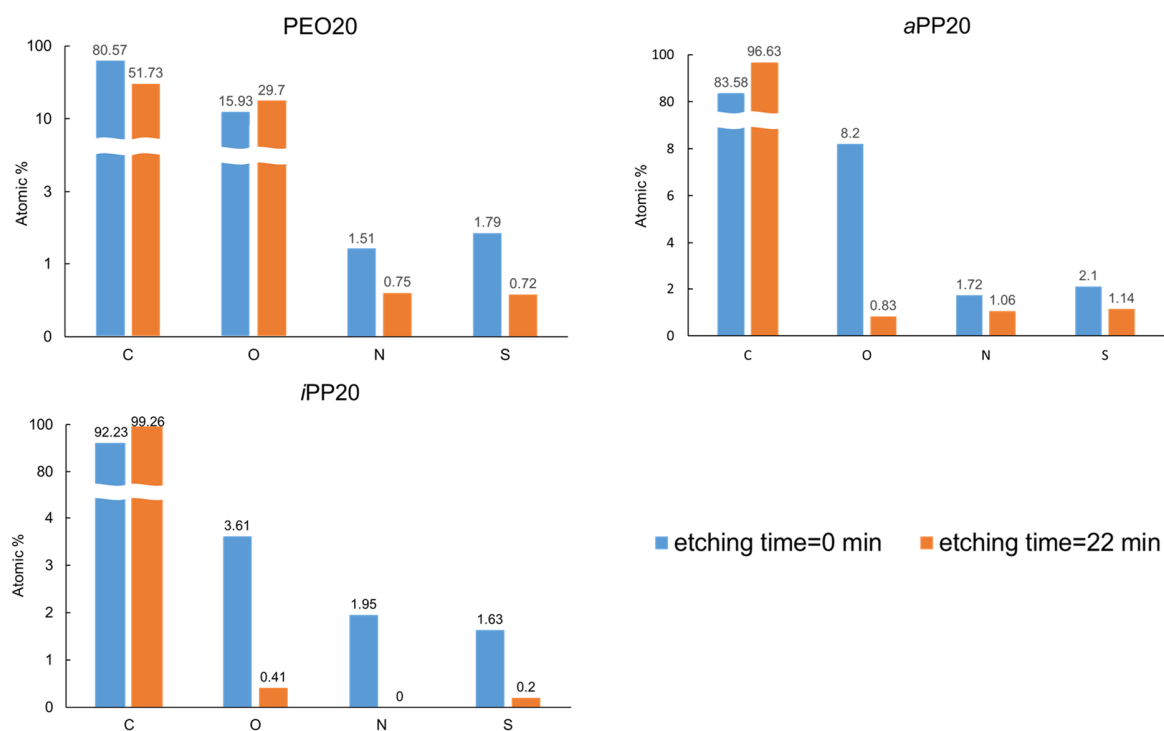
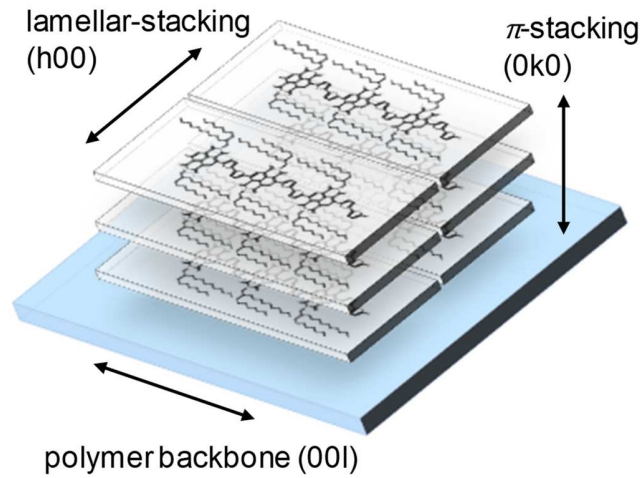


Figure S3. Elemental analysis for PEO20, aPP20, and iPP20. The blue bars indicate the results without Ar⁺ etching, while the element percentages subsequent to the Ar⁺ etching for 22 minutes are represented by the red bars.

5. GIXS data



Two-dimensional GIXS images and one-dimensional average intensity of pristine polymers are plotted. It is clear to observe the crystalline properties of PEO, *a*PP, and *i*PP (**Figure S4b–d**) in comparison to P(NDI2OD-T2) (**Figure S4a**). The diffraction signals in q_{xy} and q_z vectors are presented in **Figure S5**. The following notations describes individual vectors in accordance to reported literatures.^[1]

(a) P(NDI2OD-T2): f_1 for lamella (100) of crystallite in face-on orientation; f_2 for lamella (200) of crystallite in face-on orientation; f_3 for π -stacking (010) of crystallite in face-on orientation; b_1 for polymer backbone (001) of crystallite in face-on orientation; e_1 for lamella (100) of crystallite in edge-on orientation; e_2 for π -stacking (010) of crystallite in edge-on orientation.

(b) PEO: p_1 for (120); p_2 for (112)/(004).

(c) *a*PP: a_1 for (110); a_2 for (040); a_3 for (130); a_4 for (111).

(d) *i*PP: i_1 for (110); i_2 for (040); i_3 for (130); i_4 for (111); i_5 for (131)/(041); i_6 for (060).

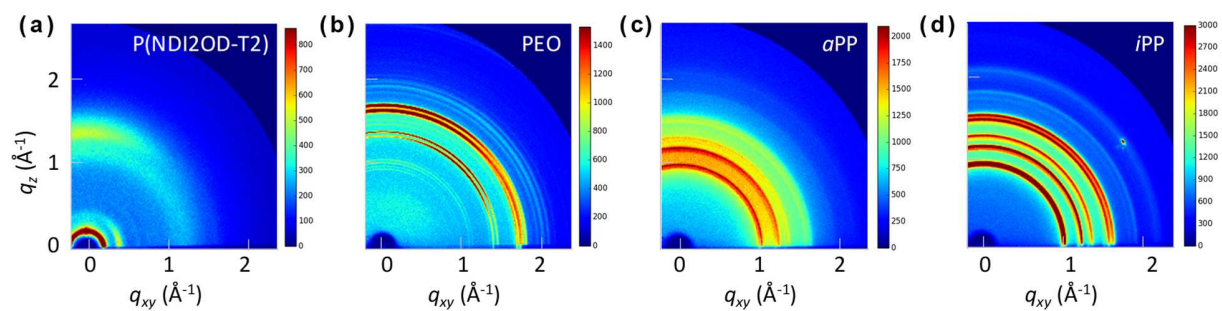


Figure S4. Two-dimensional GIXS images of neat polymers: **(a)** P(NDI2OD-T2) **(b)** PEO, **(c)** aPP, and **(d)** iPP on silicon wafers. (Annealed temperature = 110 °C)

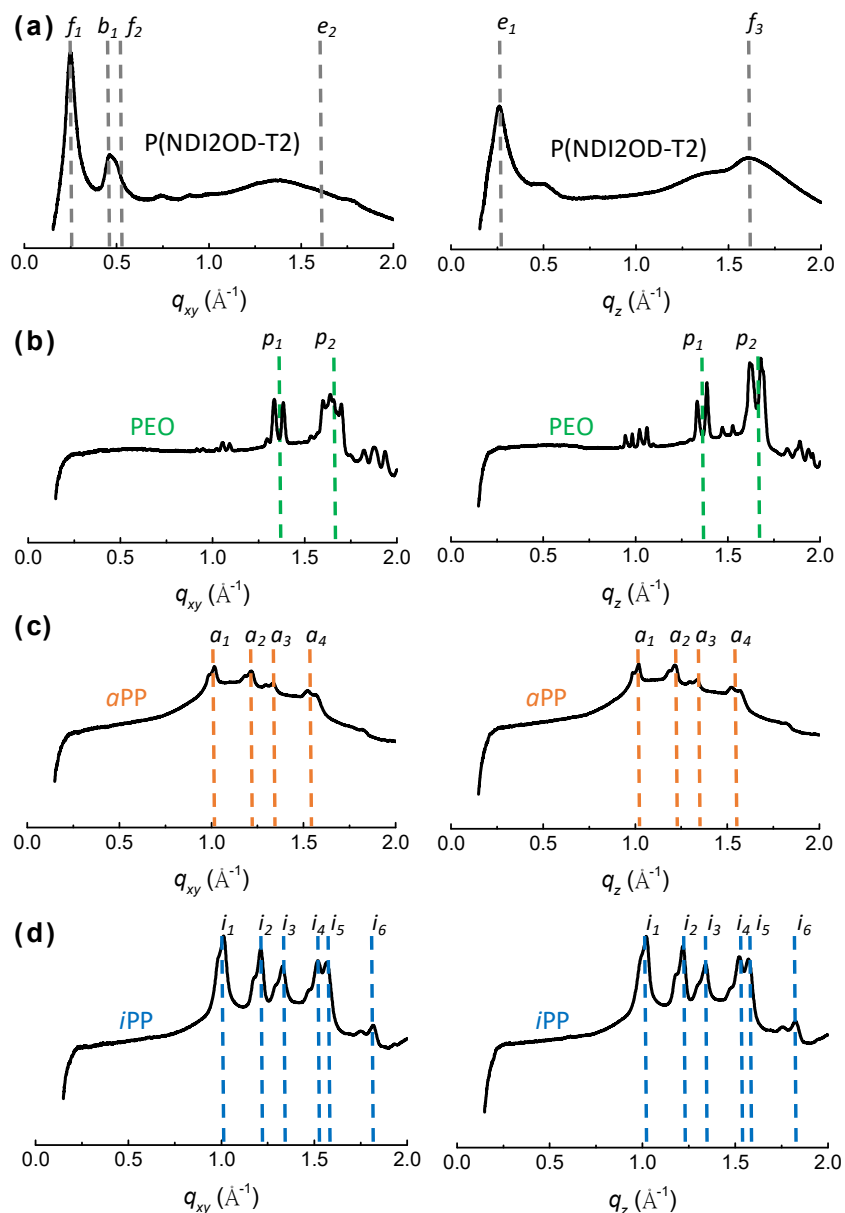


Figure S5. One-dimensional GIXS profiles of (a) P(NDI2OD-T2), (b) PEO, (c) *a*PP, and (d) *i*PP exhibiting the average intensity along q_{xy} and q_z vectors, respectively.

Similarly, two-dimensional GIXS images and the average intensity along q_{xy} and q_z vectors of the blends are summarized in **Figure S6** and **Figure S7**. For polymer blends, diffraction patterns between P(NDI2OD-T2) and PEO/ *a*PP/ *i*PP are overlapped. The individual diffraction patterns are extracted through peak-fitting via Lorentz function with a converged condition monitored by

Pearson's adjusted R^2 . Thereby, the diffraction patterns of P(NDI2OD-T2) crystallites were denoted by dash line and the extracted data are tabulated in **Table S1**.

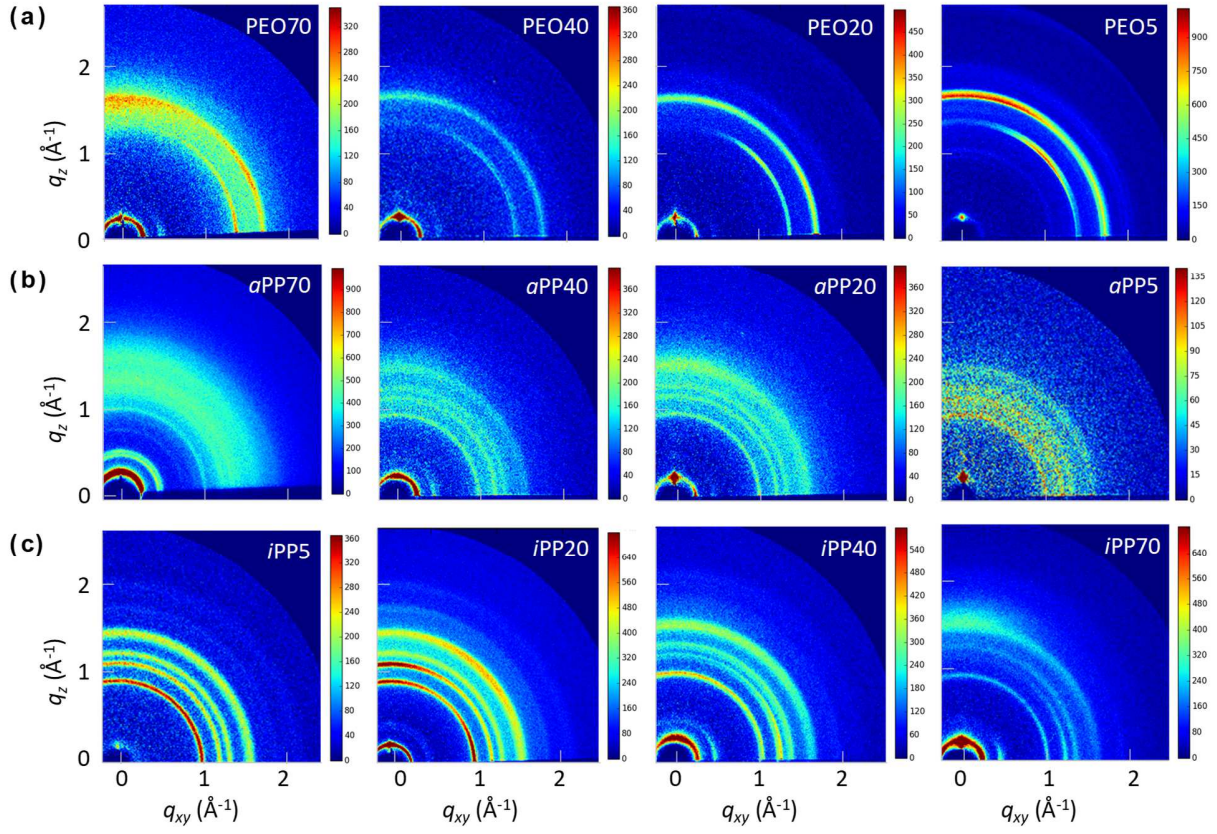


Figure S6. Two-dimensional GIXS images of **(a)** PEO blends, **(b)** *a*PP blends, **(c)** *i*PP blends on silicon wafers. (Annealed temperature = 110 °C)

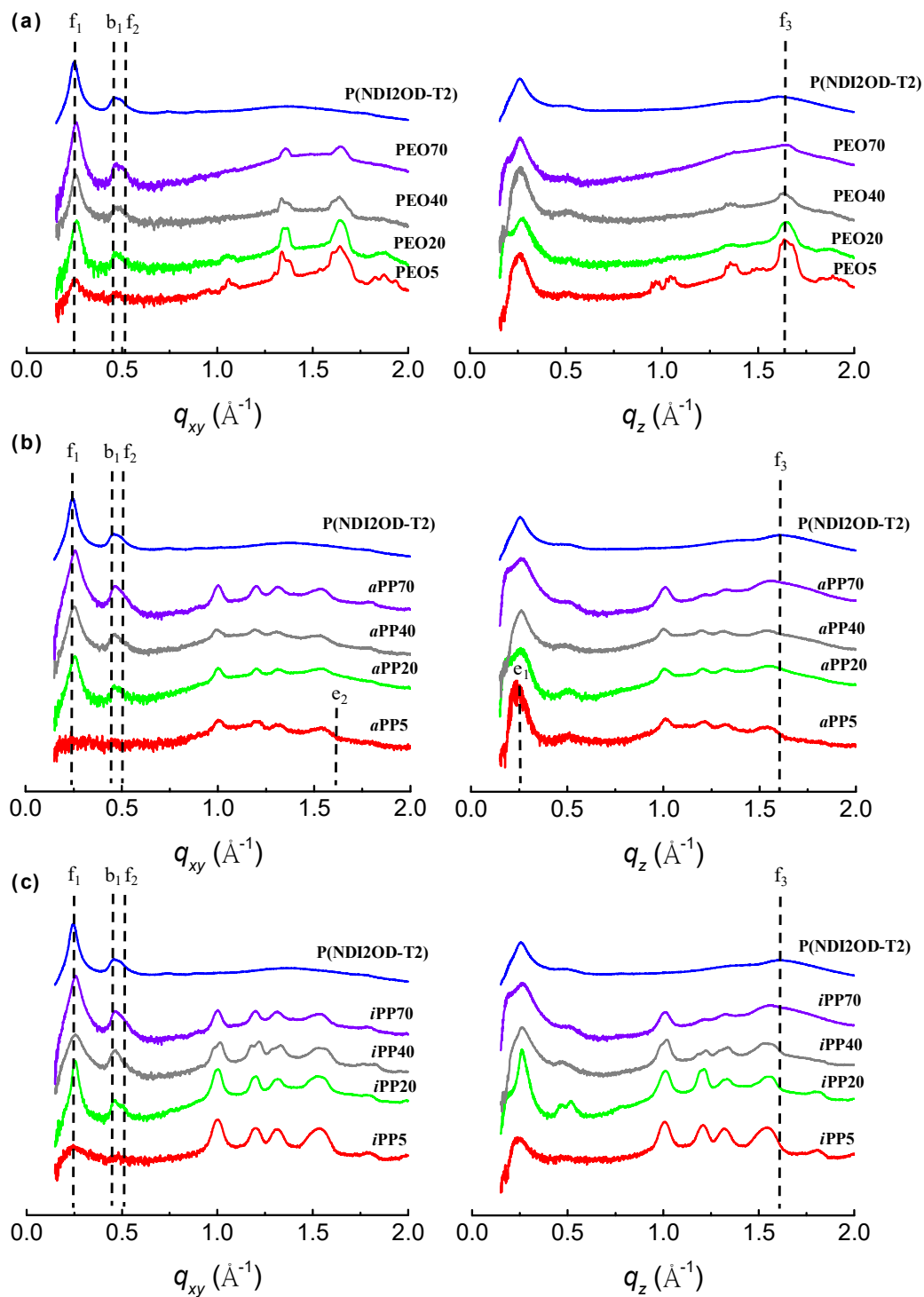


Figure S7. One-dimensional GIXS profiles of (a) PEO series, (b) *a*PP series, and (c) *i*PP series along q_{xy} and q_z vectors, respectively.

Table S1. GIXS Results for Pristine P(NDI2OD-T2) and P(NDI2OD-T2) in the Blends

Conditions	Lamellar-stacking			π -Stacking			Polymer backbone		
	d^a (Å)	$L_{c,L}$ (Å) ^{b)}	γ_L	d (Å)	$L_{c,\pi}$ (Å)	γ_π	d (Å)	$L_{c,B}$ (Å)	γ_B
PNDI	25.4	229	100%	3.9	21	100%	13.9	117	100%
PEO70	24.6	173	76%	3.9	7	35%	12.7	94	80%
PEO40	24.8	159	69%	3.9	21	99%	13.5	101	86%
PEO20	25.1	159	69%	n/a ^{c)}	0	0%	13.6	157	134%
PEO5	24.9	106	46%	n/a	0	0%	13.5	100	86%
α PP70	24.8	260	114%	3.9	9	43%	13.7	147	125%
α PP40	24.8	126	55%	3.8	16	76%	13.7	119	102%
α PP20	25.1	143	62%	n/a	0	0%	13.6	184	157%
α PP5 ^{d)}	26.0	82	36%	3.6	27	128%	n/a	0	0%
<i>i</i> PP70	24.4	137	60%	3.8	15	70%	13.6	95	82%
<i>i</i> PP40	24.4	82	36%	3.6	18	84%	13.6	104	89%
<i>i</i> PP20	24.6	228	100%	n/a	0	0%	13.7	192	164%
<i>i</i> PP5	24.5	58	25%	n/a	0	0%	n/a	0	0%

^{a)} d = d-spacing; ^{b)} L_c = coherence length; ^{c)} not applicable. ^{d)} extracted from edge-on crystallite.

6. Statistical test in $-\sigma$

The statistical tests in the deviation parameter $-\sigma$ and the two variables, γ_π and γ_B were performed. A t -test with the assumption of unequal variances as a result of a small significance F value gave a Pearson R^2 0.91, suggesting that the absorption deviation in the blends could be interpreted by both γ_B and γ_π .

Table S2. Statistical Tests Results

<i>Regression Statistics</i>				
Multiple R		0.955691919		
R Square		0.913347043		
Adjusted R Square		0.896016452		
Standard Error		0.010295684		
Observations		13		

ANOVA				
	<i>df</i>	<i>MS</i>	<i>F</i>	<i>Significance F</i>
Regression	2	0.00559	52.7014	4.886E-06
Residual	10	0.00011		

	<i>Coefficients</i>	<i>Standard Error</i>	<i>t Stat</i>	<i>P-value</i>
Intercept	-0.120834	0.008543	-14.1447	0.000000
γ_π	0.065556	0.006983	9.3875	0.000003
γ_B	0.049436	0.006524	7.5778	0.000019

7. AFM height images

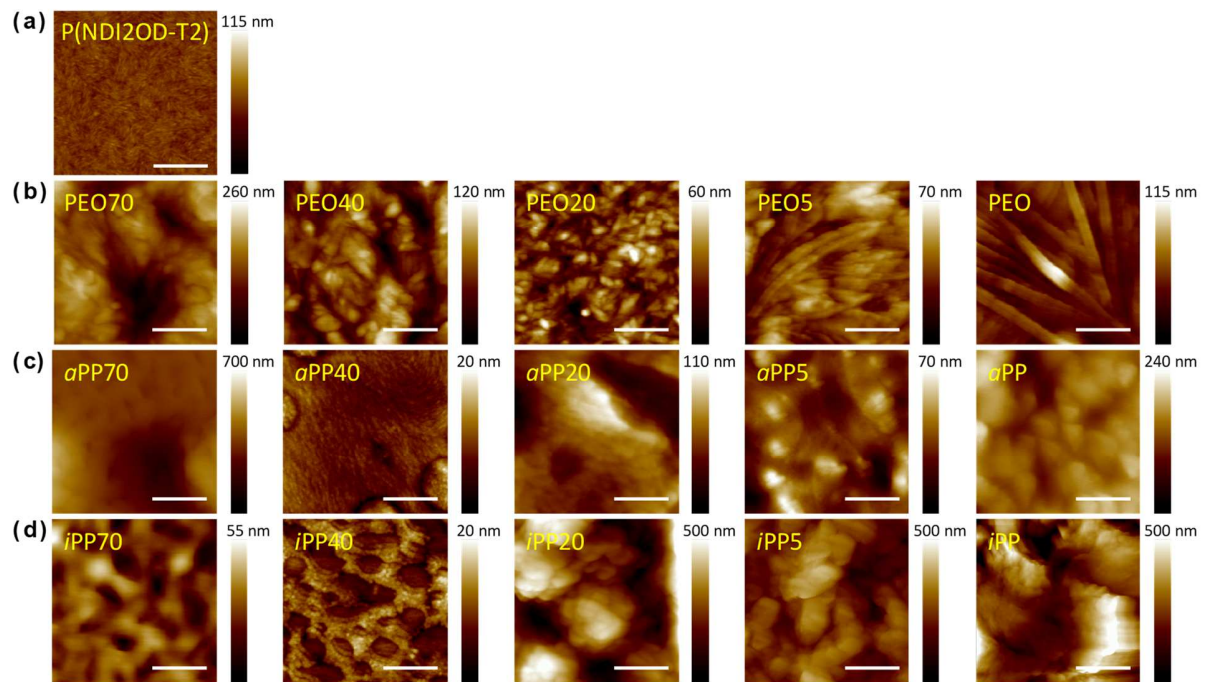


Figure S8. AFM height images (tapping-mode) of (a) neat P(NDI2OD-T2) film, (b) PEO_x, (c) *a*PP_x, and (d) *i*PP_x. The color indices are set to start from zero nm and the scale bar is 1 μm.

8. Device fabrication

Heavy n-doped silicon wafer ($1.3 \times 1.3 \text{ cm}^2$) deposited by 300 nm silicon dioxide was immersed in piranha solution ($\text{H}_2\text{SO}_4: \text{H}_2\text{O}_2 = 3: 1 \text{ v/v}$) overnight and washed with water, acetone, and isopropyl alcohol sequentially. It was treated with UV-ozone cleaner (*Jelight*) for 30 min followed by reaction with *n*-octadecyltrichlorosilane (ODTS, 5 mL) in anhydrous toluene (200 mL). Subsequent to cleaning with acetone, either polymer solution (**Table S3**) was spin-coated on top of the ODTS-modified silicon wafer. All the films were annealed at 110 °C for 1 hour. Gold (40 nm) were deposited as source and drain electrodes by thermal evaporation deposition on the semiconductor films to furnish the bottom-gate/top-contact OFET devices. The electron mobility was calculated in the saturation regime by using the equation $I_D = (\mu WC_i / 2L) \times (V_G - V_T)^2$. I_D is the drain-source current, μ is the electron mobility, W is the channel width (1000 μm), L is the channel length (100 μm), C_i (11.5 nF/cm²) is the capacitance per unit area of the gate dielectric layer, V_G is the gate voltage, and V_T is threshold voltage.

Table S3. Spin-Coating Conditions ^{a)}

Sample	Solvent	Concentration	Spin angular velocity
P(NDI2OD-T2)	Chloroform+1.5 wt% <i>o</i> -DCB	5 mg/mL	1000 rpm
PEOx	Chloroform+1.5 wt% <i>o</i> -DCB	5 mg/mL	1000 rpm
<i>o</i> PPx ^(b)	<i>o</i> -Xylene	20 mg/mL	1500 rpm
<i>i</i> PPx ^(b)	<i>o</i> -Xylene	20 mg/mL	1500 rpm

^{a)} On account of the solubility issue, it is hard to use the same spin-coating conditions for all devices. Therefore, we attempt to establish the correlation between the OFET performance and the morphological features acquired from GIXS rather than the correlation between the OFET performance and the spin-coating conditions. ^{b)} For the *o*PP or *i*PP blends, the wafers and polymer solutions were maintained at 130 °C during the course of spin coating.

9. Statistical data and transfer curves of OFETs

Table S4. Statistical Data of OFET

Conditions	μ_e (max) ^{a)} (cm ² V ⁻¹ s ⁻¹)	V_T ^{b)} (V)	I_{ON}/I_{OFF}	μ_e (avg) ^{c)} (cm ² V ⁻¹ s ⁻¹)	V_T (avg) ^{d)} (V)
P(NDI2OD-T2)	0.106	26	10 ⁵	0.065 (± 0.032) ^{e)}	23
PEO70	0.032	7	10 ⁴	0.021 (± 0.007)	-3
PEO40	0.133	21	10 ³	0.101 (± 0.019)	19
PEO20	0.041	37	10 ⁵	0.015 (± 0.013)	39
PEO5	0.003	29	10 ⁴	0.002 (± 0.001)	28
<i>a</i> PP70	0.065	7	10 ⁴	0.049 (± 0.016)	10
<i>a</i> PP40	0.063	17	10 ⁴	0.057 (± 0.006)	20
<i>a</i> PP20	0.031	-9	10 ¹	0.025 (± 0.004)	0
<i>a</i> PP5	0.127	11	10 ⁵	0.078 (± 0.030)	7
<i>i</i> PP70	0.042	23	10 ⁵	0.029 (± 0.011)	25
<i>i</i> PP40	0.044	25	10 ⁵	0.037 (± 0.006)	20
<i>i</i> PP20	0.030	24	10 ³	0.023 (± 0.005)	17
<i>i</i> PP5	0.005	9	10 ⁵	0.003 (± 0.002)	13

^{a)} Maximal electron mobility; ^{b)} Threshold voltage corresponding to maximal electron mobility; ^{c)} Average electron mobility; ^{d)} Threshold voltage corresponding to average electron mobility; ^{e)} Standard deviation with 6–20 devices.

Table S5. Statistical Tests in the μ_e^{avg} and the Two Variables, γ_π and γ_B

<i>Regression Statistics</i>	
Multiple R	0.959600113
R Square	0.920832376
Adjusted R Square	0.822726228
Standard Error	0.014732443
Observations	13

ANOVA				
	<i>df</i>	<i>MS</i>	<i>F</i>	<i>Significance F</i>
Regression	2	0.013884978	63.97284419	2.00198E-06
Residual	11	0.000217045		

	<i>Coefficients</i>	<i>Standard Error</i>	<i>t Stat</i>	<i>P-value</i>
Intercept	0	#N/A	#N/A	#N/A
γ_π	0.0583	0.0073	7.9921	6.59E-06
γ_B	0.0117	0.0046	2.5282	2.81E-02

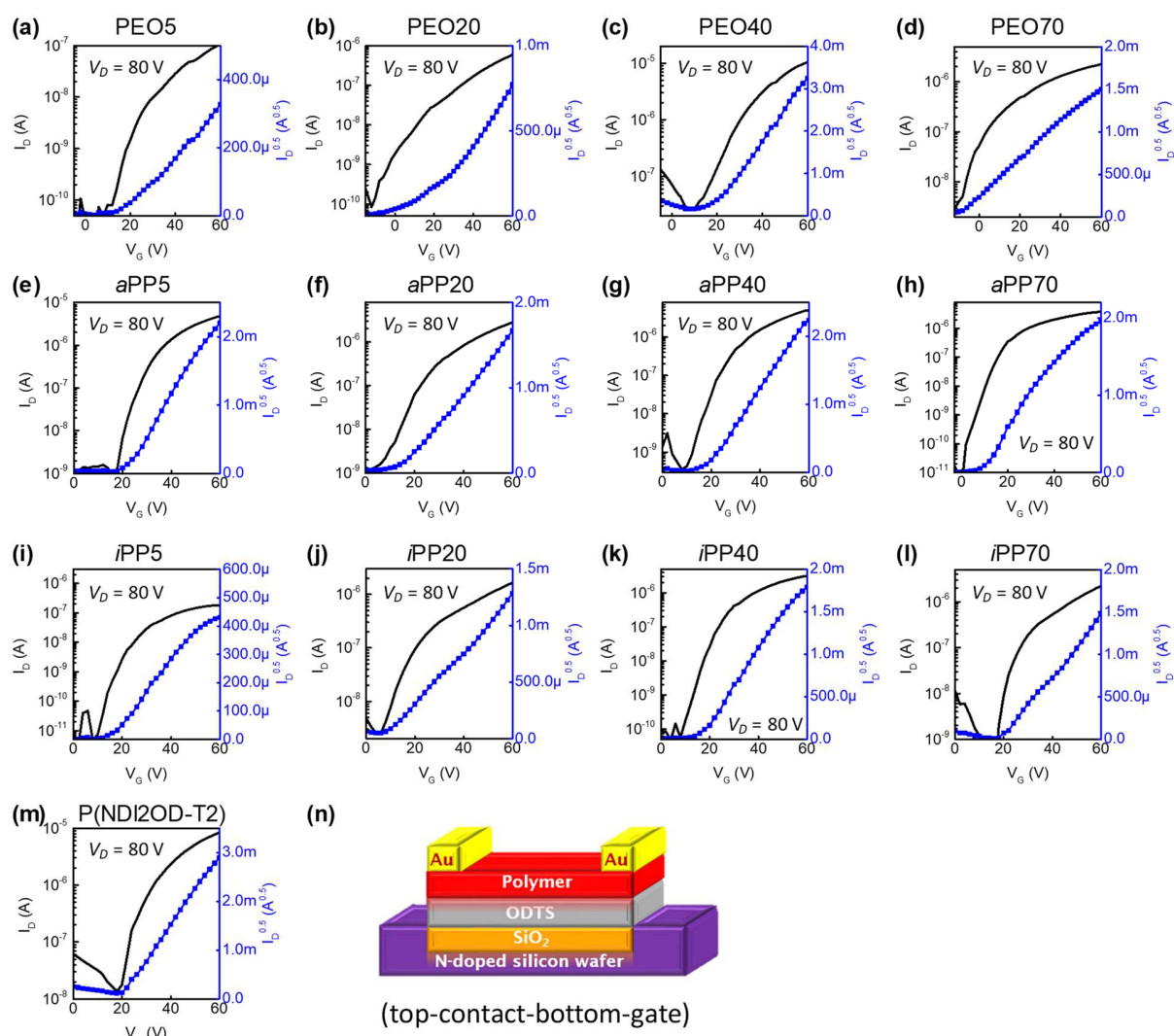


Figure S9. Representative transfer curves of top-contact/bottom-gate transistors for P(NDI2OD-T2) blended with non-conjugated polymers: PEO (a–d), aPP (e–h), and iPP (i–l) in different ratios which are signified on the top of each chart. (m) Representative transfer curve of pristine P(NDI2OD-T2). (n) Illustration for the OFET architecture.

10. Reference

- [1] a) J. E. Mark, *Physical Properties of Polymers Handbook* edited by James E. Mark, Springer Science+Business Media, LLC, New York, NY **2007**; b) T. Kuila, H. Acharya, S. K. Srivastava, B. K. Samantaray, S. Kureti, *Materials Science and Engineering: B* **2007**, 137, 217; c) K. Chrissopoulou, S. H. Anastasiadis, *European Polymer Journal* **2011**, 47, 600; d) J. Rivnay, M. F. Toney, Y. Zheng, I. V. Kauvar, Z. H. Chen, V. Wagner, A. Facchetti, A. Salleo, *Adv. Mater.* **2010**, 22, 4359.